Journal of Metals, Materials and Minerals, Vol. 33, No. 2, pp. 58-64, 2023

Synthesis of zinc oxide photocatalysts from zinc-dust waste for organic dye degradation

Wanwalee PROMSUWAN[1], Pornapa SUJARIDWORAKUN[1,2], and Wuttichai REAINTHIPPAYASAKUL[1,*]

[1] *Department of Materials Science, Faculty of Science, Chulalongkorn University, Bangkok 10330, Thailand*
[2] *Center of Excellence on Petrochemical and Materials Technology, Chulalongkorn University, Bangkok 10330, Thailand*

***Corresponding author e-mail:** wuttichai.re@chula.ac.th

Received date:
9 February 2023
Revised date
24 May 2023
Accepted date:
29 May 2023

Keywords:
Zinc oxide;
Zinc-dust waste;
Hydrothermal;
Photocatalyst;
Dye degradation

Abstract

Zinc-dust waste from a hot-dip galvanizing plant in the metal plating industry was successfully used as the starting material to synthesize zinc oxide (ZnO) nanopowder via a hydrothermal method. Effects of acid types in zinc-dust dissolving process and concentration of NaOH for precipitation on physical characteristics and photocatalytic activity of the synthesized ZnO were investigated. Elemental composition, phase and crystallite size, morphology with chemical composition, and specific surface area of the ZnO nanostructures were characterized by X-ray fluorescence spectroscopy (XRF), X-ray diffraction (XRD), scanning electron microscopy with energy dispersive X-ray spectroscopy (SEM-EDS), and gas adsorption-desorption analysis, respectively. The photocatalytic performance of the prepared ZnO was evaluated by photodegradation of rhodamine B (RhB) under UV light irradiation. The ZnO nanostructures synthesized by dissolving zinc-dust with nitric acid, then precipitating with a solution of 6 M NaOH, and hydrothermal treatment at 170°C for 8 h exhibited the highest dye degradation efficiency. It is up to 89.7% after UV irradiation for 240 min, which is comparable to the degradation efficiency of a commercial ZnO nanoparticles (92.7%). This work offers materials and synthesis method for alternative photocatalysts prepared from industrial waste that possess high photocatalytic activity for organic dye degradation.

1. Introduction

Zinc-dust waste is a product manufactured by the hot-dip galvanizing plant in metal plating industries. It is a common method for the pretreatment of steel to increase corrosion resistance and to enhance the lifetime of the materials. In the final step of this treatment, the excess zinc is removed in a form of dust containing zinc as the main constituent, leading to excessive amount of zinc-dust waste powder. Recycling or upcycling zinc-dust waste is one of the major challenges for metal plating factories. Alternatively, using zinc-dust waste powder as a starting material for the synthesis of ZnO is one of the interesting solutions. This approach is crucial for reducing waste and also raising the value of zinc-dust. Additionally, ZnO is widely applied as a photocatalyst for the decomposition of organic substances that cause water pollution issues [1-3]. ZnO photocatalytic nanoparticles are promising for environmental applications due to their exceptional properties such as easy functionalization, non-toxicity, large surface area, large number of reactive sites, high catalytic activity, good thermal and chemical stability [4,5].

In recent years, green synthesis has opened up new avenues in the scientific fields of nanomaterial engineering and catalysis, allowing the alternative preparation processes of nanomaterials with desired properties [6]. Hydrothermal treatment of ZnO nanomaterials has been reported by many researchers because it is a simple, cost-effective, and energy-efficient method for synthesizing ZnO nanomaterials with well-crystallized, uniformly-sized and shaped products at relatively low temperatures. The morphology of the obtained ZnO nanostructures could be controlled by varying parameters including concentration, reaction temperature, pH of the solution, and the presence of different capping agents [7-10].

Typically, highly purified, chemically treated and commercially available zinc salts have been used as precursors for the preparation of ZnO photocatalysts by hydrothermal treatment [11-14]. There are only few works reporting utilization of some zinc-containing industrial wastes as alternative precursors. From the previous research, Sujaridworakun *et al.* [1] studied on the preparation of ZnO particles from zinc-dust waste from hot-dip galvanizing process. The pH adjustment in a range of 8 to 12 by NaOH solutions and the addition of hydroxypropyl cellulose (HPC) dispersant were studied. The hydrothermal process was carried out at 170°C for 8 h. The ZnO particles obtained from the suspension with pH of 12 vol% and 0.10 vol% of HPC exhibited desirable photocatalytic activity under UV irradiation. With this preliminary research, there are many other parameters for the synthesis of ZnO nanostructures from zinc-dust waste by hydrothermal treatment that could be further explored. As a result, the novelty of this research is to study some important conditions of dissolving and precipitating processes for converting zinc-dust waste into ZnO photocatalysts.

In this work, zinc-dust powder from a hot-dip galvanizing plant was used as the starting material to synthesize ZnO nanostructures via a hydrothermal process. Effects of acid types for zinc-dust dissolving

process and concentration of NaOH for precipitation on physical characteristics and photocatalytic activity by organic dye degradation of the synthesized ZnO were investigated.

2. Experimental

2.1 Materials

Zinc-dust waste, obtained from a hot-dip galvanizing plant (Siam Frit Co., Ltd.), was used as the starting material. Sulfuric acid (H_2SO_4, 98%, Ajax Finechem), and nitric acid (HNO_3, 65%, EMSURE) were used for dissolution of zinc-dust waste. Sodium hydroxide (NaOH, AR grade, KEMAUS) was used for precipitation. Rhodamine B (RhB, Loba Chemie) was used as the target organic pollutant for photocatalytic activity test. Commercial ZnO nanoparticles (ZnO-Com., MTI Corporation Co., Ltd.) were used as a reference in the photocatalytic activity test. All commercial chemicals were used as received without further purification.

2.2 Synthesis of ZnO nanostructures from zinc-dust powder

2 g of zinc-dust powder was dispersed in 20 mL of deionized water and the mixture was stirred at room temperature for 10 min. Then, sulfuric acid (3.1 M) or nitric acid (4.5 M) were added to the mixture and stirred for 150 min. After that, the undissolved powder was filtered out and the clear solution was collected. Subsequently, NaOH (3 M, 6 M, 12 M) was added dropwise to the clear solution with vigorous stirring at room temperature until the mixture reached pH ~12 and white precipitate was formed. The suspension was placed in a 45 mL Teflon-lined stainless steel autoclave and was heated at 170°C for 8 h. The sample was then cooled to room temperature, and the obtained white precipitate was centrifuged, washed with deionized water and then ethanol. Finally, the white powder of ZnO was dried at 80°C overnight. The name of the prepared samples is denoted by dissolving acid type (S for sulfuric acid and N for nitric acid) and NaOH concentration using during precipitation (3 M, 6 M, and 12 M).

2.3 Characterizations

The elemental composition of zinc-dust powder and the prepared samples was analyzed using an X-ray fluorescence spectrometer (XRF; Bruker S8 Tiger). The crystal structure and crystalline phase of zinc-dust powder and the prepared photocatalysts was determined using X-ray diffraction (XRD) by an X-ray diffractometer (Bruker, D8 Advance) with a Cu K_α radiation source. XRD patterns were taken from a 5° to 80° (2θ) range. The crystallite size was calculated using the Scherrer equation by equation (1)

$$D = k\lambda/\beta \cos\theta \quad (1)$$

where D is the average crystallite size (nm), k is the dimensionless shape factor = 0.9, λ is the X-ray wavelength = 0.15406 (nm), β is the full-width at half maximum (radians), and θ is the Bragg-diffraction angle (radians) [15].

Morphology and microstructure with chemical composition were obtained using a scanning electron microscopy with energy dispersive X-ray spectroscopy (SEM-EDS; JEOL-JSM-6840LV) at 20 kV. The dimension of the particles was calculated using the ImageJ program. The specific surface area, pore size, and pore volume of the prepared photocatalysts was analyzed using a surface area and porosimetry analyzer (Micromeritics, 3Flex 3500). Brunauer-Emmett-Teller (BET) isotherm with nitrogen gas adsorption analysis was used to compute the specific surface area.

2.4 Photocatalytic activity evaluation

The photocatalytic activity of the synthesized powders was evaluated by photodegradation of RhB solution under UV light source (Blacklight lamp 18 W, 980 $\mu W \cdot cm^{-2}$). RhB is chosen for photocatalytic degradation test because it is a common dye that is used extensively in industries related to plastic, leather, cosmetics, and textiles, etc. This dye is an organic contaminant that damages the environment and harms both human health and the biological balance [1]. Due to chemical stability and photostability of RhB, its degradation process is challenging. Under photocatalytic degradation process of RhB, UV light is selected to be a light source because the wavelength of the UV light is corresponding to the energy band gap of ZnO (3.2 eV to 3.5 eV) [2-3].

The prepared ZnO catalysts (0.05 g) were dispersed in 120 mL of RhB solution (10 ppm) by ultrasonication for 5 min. Prior to light irradiation, the suspension was stirred in the dark for 30 min to achieve adsorption-desorption equilibrium. During dark condition, 5 mL of the solution were collected every 10 min. After UV light irradiation, 5 mL of the solution were collected every 40 min. The concentrations of the collected solutions were then determined by measuring the absorbance at the wavelength of 554 nm with a five-point standard calibration curve using a UV-Vis spectrophotometer (Perkin Elmer Lambda 35). The dye degradation efficiency (DD%) was calculated using Equation (2).

$$DD\% = [(C_0\text{-}C)/C_0] \times 100 \quad (2)$$

where C_0 represents the initial RhB concentration, and C represents the RhB concentration collected at each irradiated time [12]. The dye adsorption efficiency (DA%) of RhB on the catalysts was calculated using Equation (3)

$$DA\% = [(C_0\text{-}C_A)/C_0] \times 100 \quad (3)$$

where C_A represents the RhB concentration collected under dark condition.

3. Results and discussion

3.1 Characterization of zinc-dust powder

Elemental composition, crystalline phase, and microstructure of the zinc dust powder generated from the hot-dip galvanizing plant were characterized by XRF, XRD, and SEM, respectively. According to Table 1, XRF results show that zinc-dust powder composes of

mainly ZnO (93.86 wt%), Al_2O_3 (3.57 wt%), and trace amounts of some other metal oxides such as CuO, MgO, PbO, and SiO_2 (all combined for 2.57 wt%). This strongly suggests that zinc-dust powder is a good precursor for the synthesis of ZnO photocatalysts.

The XRD pattern of zinc-dust powder is exhibited in Figure 1. It presents characteristic peaks of ZnO hexagonal wurtzite phase at $2\theta = 31.7°$, 34.5°, 36.2°, 47.5°, 56.5°, 62.8°, 66.4°, 67.9°, 69.2°, 72.5°, and 77.0° corresponding to the (100), (002), (101), (102), (110), (103), (200), (112), (201), (004), and (202) planes, respectively [15]. In addition, characteristic peaks of copper oxide (CuO) at $2\theta = 38.0°$ and alumina (Al_2O_3) at $2\theta = 43.9°$ are shown with relatively low intensity in the XRD pattern of zinc-dust powder [16,17]. This is consistent with elemental composition by XRF analysis and indicates that phases of zinc-dust powder are mostly in forms of metal oxides.

The morphology of zinc-dust powder was investigated by SEM, as shown in Figure 2. According to the SEM image, various types of microstructures including plates, rods, needles, whiskers, and some irregular particles are presented. This is possibly due to the mixture of different phases of metal oxides and some impurities that were fabricated by non-controlled conditions.

The characterization results indicate that zinc-dust powder could be a promising alternative raw material for the synthesis of nanosized ZnO photocatalysts. However, impurities and non-uniformed particle morphology may affect their photocatalytic activity. To overcome those drawbacks, proper conditions for purification and preparation of ZnO nanostructures would be considerably studied.

3.2 Synthesis of ZnO nanostructures from zinc-dust powder

As mentions above, zinc-dust powder not only contains ZnO, but also consists of various metal oxides. In order to separate ZnO from some other metal oxides, acid dissolution is an effective method. In this work, the aqueous solutions of sulfuric acid or nitric acid were used to dissolve zinc-dust powder. The grey powder of zinc-dust was mixed into acid solutions with the controlled pH about 5, which ZnO could be dissolved completely into Zn^{2+} [18]. After removing undissolved powder, the pH of acid solutions containing Zn^{2+} were adjusted to 12 by adding NaOH solutions with different concentrations. At pH ~12, the mixture of zinc hydroxide complexes including $Zn(OH)_2$, $Zn(OH)_3^-$, and $Zn(OH)_4^{2-}$ was formed as white precipitates dispersed in the suspension [18]. To control size and shape of the synthesized particles, hydrothermal treatment was selected to prepare ZnO nanostructures. This approach is also relatively low energy consumption and environmentally-friendly method. Typically, several factors such as precursors, additives, concentration, pH, temperature, and reaction time play important roles under hydrothermal conditions. Sujaridworakun *et al.* discussed the effects of precipitation pH and additives on the preparation of ZnO nanoparticles from zinc-dust waste by hydrothermal treatment [1]. This work aims to study effects of acid types for dissolving zinc-dust powder and concentration of NaOH during precipitation on characteristics and photocatalytic activity of the synthesized ZnO nanostructures. All the prepared ZnO photocatalysts appear as white powder. Compared to using sulfuric acid as leaching solution, the samples dissolved by nitric acid exhibited higher yields of the obtained ZnO powder.

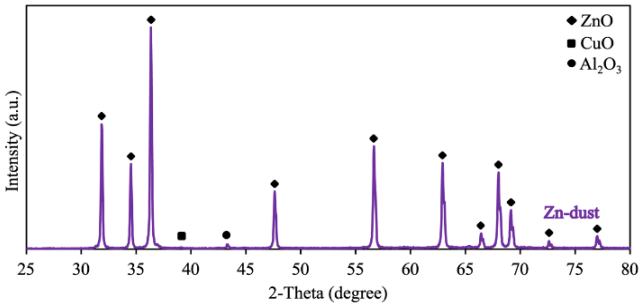

Figure 1. XRD pattern of zinc-dust powder.

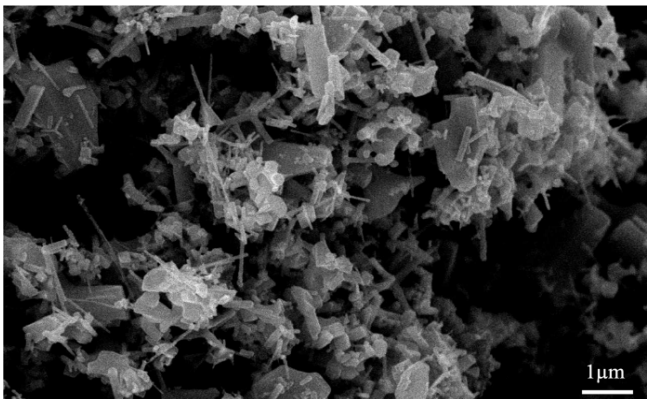

Figure 2. SEM image of zinc-dust powder.

Table 1. XRF analysis of zinc-dust powder.

Sample	Composition (wt%)					
	ZnO	**Al_2O_3**	**CuO**	**MgO**	**PbO**	**SiO_2**
Zinc-dust	93.86	3.57	0.84	0.80	0.27	0.34

Table 2. XRF analysis of ZnO photocatalysts synthesized from zinc-dust powder.

Sample	Composition (wt%)				
	ZnO	**SiO_2**	**PbO**	**CuO**	**Others**
ZnO(S-12M)	99.0	0.49	0.21	0.12	0.18
ZnO(N-12M)	98.9	0.55	0.24	0.12	0.19
ZnO(N-6M)	99.6	0.08	0.18	0.13	0.01
ZnO(N-3M)	99.3	0.26	0.21	0.13	0.10

3.3 Characterization of ZnO nanostructures synthesized from zinc-dust powder

Elemental compositions of various ZnO photocatalysts synthesized from zinc-dust powder by dissolving in sulfuric or nitric acid solutions and then precipitating with NaOH solutions at concentrations of 3 M, 6 M, and 12 M are demonstrated in Table 2. All samples exhibit high composition of ZnO (over 98.9 wt%), indicating that these hydrothermal processes are highly efficient for the preparation of ZnO photocatalysts. ZnO(N-6M) possesses the highest ZnO composition with 99.6 wt%. However, there are no significant differences incomposition of synthesized photocatalysts using different type of acids for dissolution and different NaOH concentration for precipitation.

The XRD patterns of the synthesized ZnO photocatalysts are shown in Figure 3. All the samples exhibited the same XRD diffraction pattern, which is consistent to the characteristic pattern of hexagonal wurtzite ZnO [15]. It is also the same XRD pattern predominantly found in zinc-dust powder. In contrast to zinc-dust powder, the synthesized samples present no signals of any other metal oxides in their XRD patterns. According to the Scherrer equation, the crystallite sizes of zinc-dust powder, ZnO(S-12M), ZnO(N-12M), ZnO(N-6M), and ZnO(N-3M) were around 43.20, 35.71, 33.51, 34.53, and 31.51 nm, respectively. It is noteworthy to point out that the crystallite size of synthesized ZnO is significantly reduced, compared to that of zinc-dust powder. The XRF and XRD results confirm that these synthetic approaches can effectively transform zinc-dust powder into ZnO particles with higher purity and smaller crystallite size.

The morphology of zinc-dust powder and synthesized ZnO photocatalysts were investigated by SEM, as demonstrated in Figure 4. The average dimension of synthesized ZnO photocatalysts were reported in Table 3. The SEM images of ZnO(S-12M) and ZnO (N-12M) (Figure 4(a-b)) clearly show rod-shaped structure of ZnO with relatively large diameter and length. The particle size of ZnO dissolved by nitric acid is slightly smaller than that of ZnO dissolved by sulfuric acid. The dimension of rod particles is considerably changed by altering the concentrations of NaOH. Among all the samples, rod-shaped particles of ZnO(N-6M) (Figure 4(c)) present the lowest average diameter and the shortest average length. Additionally, EDS analysis of ZnO(N-6M) (Figure 4(e)) verifies a high purity of the prepared ZnO by only detecting the distinctive peaks of Zn and O without any signals of other contaminating elements.

The specific surface area, pore size, and pore volume of the prepared samples were characterized by nitrogen gas adsorption-desorption isotherms, as depicted in Figure 5 and reported in Table 4. According to the adsorption-desorption isotherms, all the synthesized ZnO photocatalysts possess Type IV adsorption-desorption isotherms, indicating mesoporous solid structures. From Table 4, the BET specific surface areas of ZnO(S-12M), ZnO(N-12M), ZnO(N-6M), and ZnO(N-3M) are 6.94, 6.14, 9.59, 4.45 $m^2 \cdot g^{-1}$, respectively. The results reveals that the ZnO(N-6M) exhibits the highest specific surface area and all the samples have pore size and pore volume in the same range.

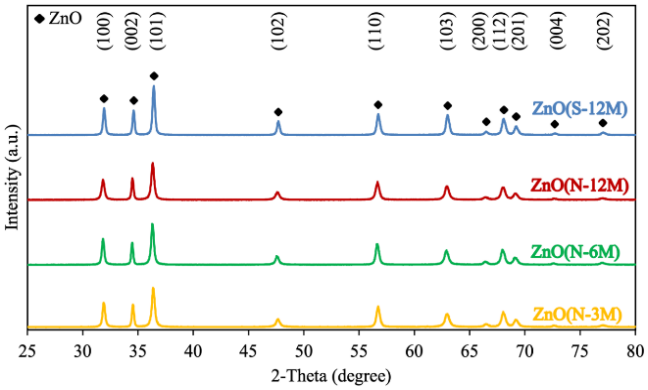

Figure 3. XRD patterns of ZnO photocatalysts synthesized from zinc-dust powder by hydrothermal process.

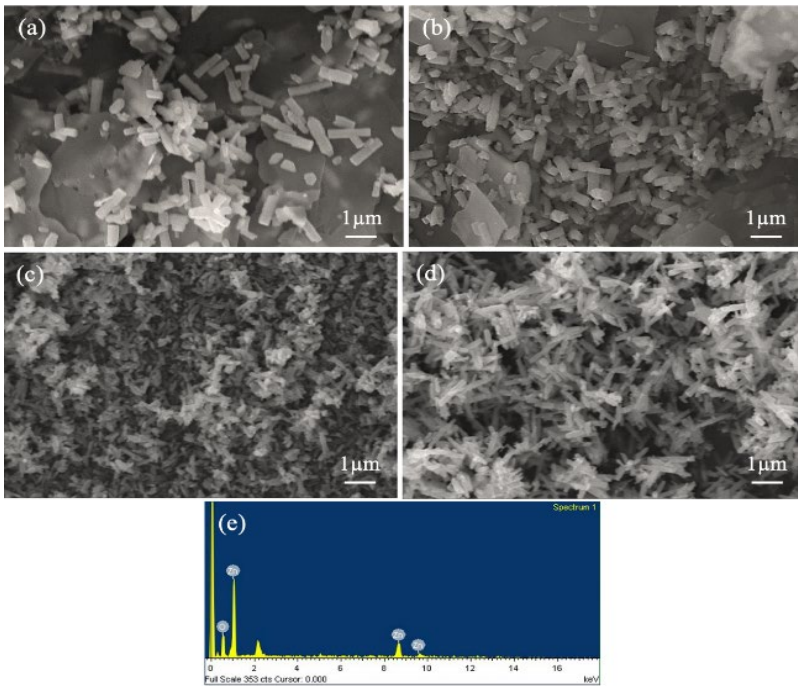

Figure 4. SEM image of (a) ZnO(S-12M), (b) ZnO(N-12M), (c) ZnO(N-6M) (d) ZnO(N-3M), and (e) EDS analysis of a rod structure in ZnO(N-6M).

Table 3. The average particle dimension in diameter, length, and aspect ratio of ZnO photocatalysts synthesized from zinc-dust powder.

Sample	Diameter (μm)	Length (μm)	Aspect Ratio
ZnO(S-12M)	0.32	1.07	3.34
ZnO(N-12M)	0.25	0.75	3.00
ZnO(N-6M)	0.14	0.41	2.93
ZnO(N-3M)	0.19	0.74	3.89

Table 4. Specific surface area (S_{BET}), pore size, and pore volume of ZnO photocatalysts synthesized from zinc-dust powder.

Sample	S_{BET} ($m^2 \cdot g^{-1}$)	Average pore size (nm)	Average pore volume ($cm^3 \cdot g^{-1}$)
ZnO(S-12M)	6.94	7.32	0.0254
ZnO(N-12M)	6.14	6.44	0.0607
ZnO(N-6M)	9.59	7.21	0.0301
ZnO(N-3M)	4.45	7.05	0.0416

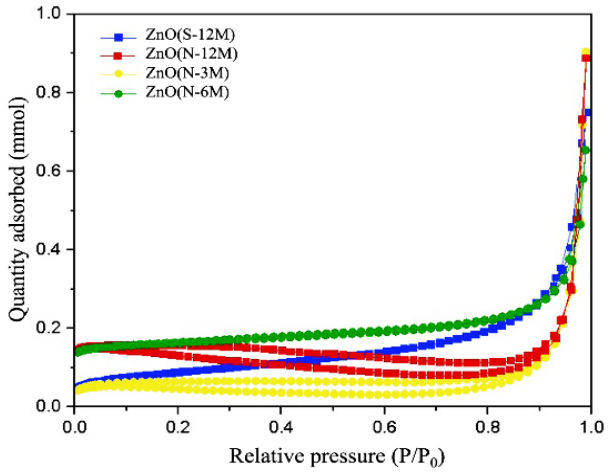

Figure 5. Nitrogen gas adsorption–desorption isotherms of ZnO photocatalysts synthesized from zinc-dust powder.

3.4 Photocatalytic activity evaluation

The photocatalytic activity of various ZnO photocatalysts were evaluated by the photodegradation of RhB dye solution under UV irradiation. The correlation between C/C_0 and irradiation time of RhB, ZnO-Com., zinc-dust powder, and synthesized ZnO photocatalysts under UV irradiation for 240 min is shown in Figure 6. In the absence of photocatalysts, the pristine RhB dye solution clearly exhibited no degradation during the test period, reflecting the high stability of RhB under UV irradiation. On the other hand, the degradation of RhB was observed as the presence of ZnO photocatalysts in the suspension. The absorption of UV light excites electrons from valence band (VB) to conduction band (CB), creating the electron-hole pairs. Subsequently, they enable generation of reactive oxygen species (ROS) including superoxide and hydroxyl radicals on the surface, which are useful for degradation of organic pollutants in water. To achieve high photocatalytic performance, a photocatalyst requires an appropriate band gap for harvesting light, facile separation and transportation of electrons and holes, and proper valence band and conduction band edge potential for redox reaction being thermodynamically feasible [19].

As illustrated in Figure 6, ZnO-com. shows the best photocatalytic activity due to its spherical particles with size of about 50 nm and high specific surface area of 33.95 $m^2 \cdot g^{-1}$. Both ZnO(S-12M) and ZnO(N-12M) exhibit similar RhB photodegradation rate, which is obviously not efficient compared to that of zinc-dust powder. This indicates that using too high concentration of NaOH for precipitation results in relatively large microstructure of ZnO and low photocatalytic activity. On the other hand, ZnO(N-6M) and ZnO(N-3M) exhibit better RhB photodegradation rate compared to that of zinc-dust powder. Among all the synthesized samples, ZnO(N-6M) photocatalyst achieves the best photocatalytic activity for RhB degradation. It is possibly because of its microstructure and higher specific surface area.

The efficiencies of dye degradation (DD%) and dye adsorption (DA%) of ZnO-Com., zinc-dust powder, and synthesized ZnO photocatalysts under UV irradiation for 240 min are summarized in Figure 7. Zinc-dust powder and all the synthesized ZnO photocatalysts contain the similar DA% due to their similar specific surface area. On the other hand, ZnO-com. has slightly higher DA% compared to others, thanks to its significantly higher specific surface area. The DD% under UV light irradiation for 240 min of ZnO-Com., zinc-dust powder, ZnO(S-12M), ZnO(N-12M), ZnO(N-6M), and ZnO(N-3M) are 92.7, 74.2, 50.7, 55.0, 89.7, and 83.0%, respectively. The DD% of ZnO(N-6M) is considerably comparable to that of ZnO-com. This indicates that the ZnO nanostructures prepared from zinc-dust powder waste dissolved in nitric acid solution, precipitated with 6 M NaOH and treated by hydrothermal process could be a good candidate for using as a highly effective ZnO photocatalyst.

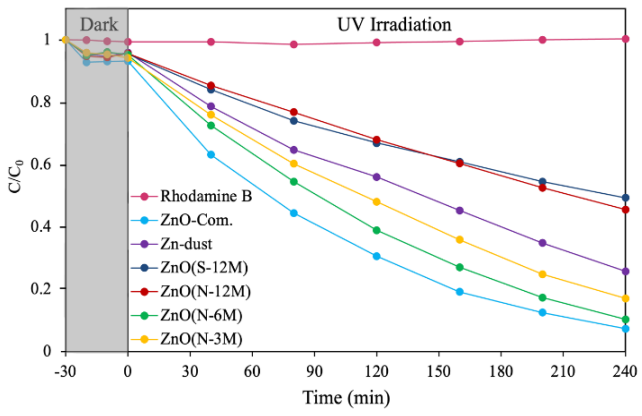

Figure 6. The correlation between C/C_0 and irradiation time of RhB, ZnO-Com., zinc-dust powder, and synthesized ZnO photocatalysts under UV irradiation for 240 min.

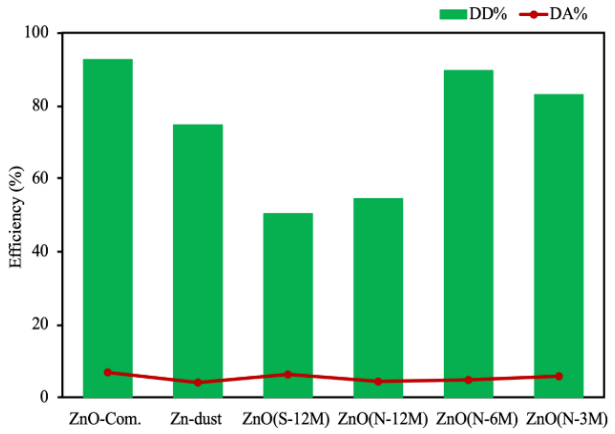

Figure 7. The efficiencies of dye degradation (DD%) and dye adsorption (DA%) of ZnO-Com., zinc-dust powder, and synthesized ZnO photocatalysts under UV irradiation for 240 min.

4. Conclusions

ZnO photocatalysts were successfully synthesized from Zn-dust waste by hydrothermal method. The type of acid used for zinc-dust dissolution and the concentration of NaOH used for precipitation on photocatalytic activity of the synthesized ZnO nanostructures were studied. Among all the synthesized samples, the ZnO photocatalysts prepared by dissolving zinc-dust with nitric acid, precipitating with a solution of 6 M NaOH, and hydrothermal treatment at 170°C for 8 h showed the best photodegradation rate of RhB under UV irradiation. Its photocatalytic activity is comparable to that of commercial ZnO nanoparticles. In summary, this work successfully presents the synthesis method for converting zinc-dust waste powder into ZnO nanostructures as highly UV-effective photocatalysts for organic dye degradation.

Acknowledgements

This research project was financially supported by Office of the Permanent Secretary, Ministry of Higher Education, Science, Research and Innovation. It was partially supported by grants for development of new faculty staff, Ratchadaphiseksomphot Fund, Chulalongkorn University. The authors also would like to thank Department of Materials Science, Faculty of Science, Chulalongkorn University and staffs for the research facilities and characterization supports.

References

[1] P. Sujaridworakun, and K. Natrchalayuth, "Influence of pH and HPC concentration on the synthesis of zinc oxide photocatalyst particle from zinc-dust waste by hydrothermal treatment," *Advanced Powder Technology,* vol. 25, pp. 1266-1272, 2014.

[2] W. Liu, M. Wang, C. Xu, and S. Chen, "Facile synthesis of g-C_3N_4/ZnO composite with enhanced visible light photooxidation and photoreduction properties," *Chemical Engineering Journal,* vol. 209, pp. 386-393, 2012.

[3] X. Tan, X. Wang, H. Hang, D. Zhang, N. Zhang, Z. Xiao, and H. Tao, "Self-assembly method assisted synthesis of g-C_3N_4/ZnO heterostructure nanocomposites with enhanced photocatalytic performance," *Optical Materials,* vol. 96, p. 109266, 2019.

[4] G. Kamarajan, D. Benny Anburaj, V. Porkalai, A. Muthuvel, and G. Nedunchezhian, "Green synthesis of ZnO nanoparticles using Acalypha indica leaf extract and their photocatalyst degradation and antibacterial activity," *Journal of the Indian Chemical Society,* vol. 99, p. 100695, 2022.

[5] O. Eskikaya, S. Ozdemir, G. Tollu, N. Dizge, R. Ramaraj, A. Manivannan, and D. Balakrishnan, "Synthesis of two different zinc oxide nanoflowers and comparison of antioxidant and photocatalytic activity," *Chemosphere,* vol. 306, pp. 135389, 2022.

[6] A. Ashar, I. A. Bhatti, T. Siddique, S. M. Ibrahim, S. Mirza, Z. A. Bhutta, M. Shoaib, M. Ali, M. B. Taj, M. Iqbal, S. Noor, and M. Mohsin, "Integrated hydrothermal assisted green synthesis of ZnO nano discs and their water purification efficiency together with antimicrobial activity," *Journal of Materials Research and Technology,* vol. 15, pp. 6901-6917, 2021.

[7] N. S. Ridhuan, K. A. Razak, Z. Lockman, and A. A. Aziz, "Structural and morphology of ZnO nanorods synthesized using ZnO seeded growth hydrothermal method and its properties as UV sensing," *PLOS ONE,* vol. 15, p. 50405, 2012.

[8] O. Lupan, and T. Pauporte, "Hydrothermal treatment for the marked structural and optical quality improvement of ZnO nanowire arrays deposited on light weight flexible substrates," *Journal of Crystal Growth,* vol. 312, pp. 2454-2458, 2010.

[9] V. Gerbreders, M. Krasovska, E. Sledevskis, A. Gerbreders, I. Mihailova, E. Tamanis, and A. Ogurcovs, "Hydrothermal synthesis of ZnO nanostructures with controllable morphology change," *Royal Society of Chemistry,* vol. 22, pp. 1346-1358, 2022.

[10] X. Chen, A. M. C. Ng, A. B. Djurisic, C. C. Ling, and W. K. Chan, "Hydrothermal treatment of ZnO nanostructures," *Thin Solid Films,* vol. 520, pp. 2656-2662, 2012.

[11] P. Lad, V. Pathak, A. B. Thakkar, P. Thakor, M. P. Deshpande, and S. Pandya, "ZnO nanoparticles synthesized by precipitation method for solar-driven photodegradation of methylene blue dye and its potential as an anticancer agent," *Brazilian Journal of Physics,* vol. 53, p. 63, 2023.

[12] R. P. Cuapio, J. A. Alvarado, H. Juarez, and H-J. Sue, "Sun irradiated high efficient photocatalyst ZnO nanoparticles obtained by assisted microwave irradiation," *Materials Science and Engineering,* vol. 289, p. 116263, 2023.

[13] S. Sheikhi, M. Aliannezhadi, and F. S. Tehrani, "The effect of PEGylation on optical and structural properties of ZnO nanostructures for photocatalyst and photodynamic applications," *Materials Today,* vol. 34, p. 105103, 2023.

[14] S. N. Q. A. A. Aziz, K. C. Meng, S. Y. Pung, Z. Lockman, A. U. Hamid, and W. K. Tan, "Rapid growth of zinc oxide nanorods on kanthal wires by direct heating method and its photocatalytic performance in pollutants removal," *Journal of Industrial and Engineering Chemistry,* vol. 118, pp. 226-238, 2023.

[15] T. M. Elmorsi, M. H. Elsayed, and M. F. Bakr, "Enhancing the removal of methylene blue by modified ZnO nanoparticles: kinetics and equilibrium studies," *Journal of Chemistry,* vol. 95, pp. 590-600, 2017.

[16] S. M. Ambalagi, M. Devendrappa, S. Nagaraja, and S. Sannakki, "Dielectric properties of PANI/CuO nanocomposites," *Materials Science and Engineering,* vol. 310, p. 012081, 2018.

[17] K. Zhao, B. Cao, J. Liu, Y. Wang, and L. An, "In-situ synthesis of Al76.8Fe24 complex metallic alloy phase in Al-based hybrid composite," *Journal of Materials Science & Technology,* vol. 33, pp. 1177-1181, 2017.

[18] A. Degen, and N. Kosec, "Effect of pH and impurities on the surface charge of zinc oxide in aqueous solution," *Journal of the European Ceramic Society,* vol. 20, pp. 667-673, 2000.

[19] K. Rupiyawet, K. Kaewlob, P. Sujaridworakun, P. Buggakupta, "Optimization of mixing conditions on the physical and tribological properties of brake pads" *Key Engineering Materials*, vol. 824, pp. 67-72, 2019.